Investigating the Robustness of Disentangled Variational Autoencoders to Adversarial Examples

Sten Sootla[1]

Computational Statistics and Machine Learning

Supervised by Dr. Cristina Calnegru and Dr. John Shawe-Taylor

Submission date: 10.08.2018

Abstract

Summarise your report concisely.

Contents

1 Introduction **2**

2 Related work and background **4**

2.1 Probabilistic learning and inference 4

2.1.1 Discriminative approach 4

2.1.2 Generative approach 5

2.2 Variational autoencoders 8

2.2.1 General framework 8

2.2.2 Specific example 10

2.2.3 Incorporating discrete variables 11

2.3 Disentangled representations 13

2.4 Adversarial examples 13

3 Methods **14**

4 Results **15**

5 Conclusion **16**

6 Appendix **17**

Chapter 1

Introduction

In recent years, deep neural networks have shown impressive results in various supervised pattern recognition tasks, including image classification [20, 15], object detection [12], and machine translation [2]. Capitalizing on the resurgence of deep neural models in the supervised learning domain, unsupervised methods have also gone through a renaissance, as they have moved from modelling relatively simple toy datasets to being able to capture exceedingly complex real-world distributions [4, 27]. One of the most prominent generative models behind these successes is the variational autoencoder (VAE) [19], which merges conventional probabilistic methods with deep learning, using neural networks to parameterize both the generative and approximate posterior distributions in the the evidence lower bound.

The successes of these models, which mainly consist of stacks of layers, each of which is composed of a linear mapping followed by a nonlinearity, can be attributed to the fact that they can theoretically approximate arbitarily complex functions [7]. However, as the appropriate functions are discovered automatically via a black-box optimization algorithm (e.g. gradient descent or an evolutionary method), the models can have counter-inuitive properties [28].

First, the resulting decision boundaries of the trained networks are often non-interpretable and unintuitive. Indeed, one of the most well-known and intriguing failure modes of most machine learning algorithms is the existence of adversarial examples - datapoints that are perceptually very close to examples from the original training distribution, but which fool the model with high confidence [28]. The fact that state-of-the-art deep learning models are subject to such adversarial perturbations challenges the narrative that they are unreasonably effective in generalizing outside the distribution they are trained on. More practically, as the models under discussion are being pushed into production for use in semi-autonomous vehicles [6], drones [25], surveillance cameras [9] and malware detection pipelines [14], the existence of adversarial examples poses a security threat with possible real-world consequences.

Second, the internal representations learnt by deep neural networks are infamously complex and hard to analyse, giving them a reputation of being completely black-box learning machines. Indeed, Szegedy et. al. [28] have shown that directions along the coordinate axes are often no more

semantically meaningful than other directions in the latent space, while Morcos et. al. [24] discovered that even if there exist individual units that are interpretable, they are no more important to the task at hand than neurons that don't exhibit clear correlation with specific semantic concepts. In other words, the models learn representations where units are *entangled* - each individual semnatically meaningful factor of variation in the input is explained by a combination of units, as opposed to a single neuron.

It has been argued [3] that such entangled representations are suboptimal for generalization, and incorporating inductive biases which would steer the representations towards *disentanglement* would be beneficial. Indeed, it seems intuitively plausible that generalizing to novel configuration of concepts that was not encountered in the training distribution is easiest when relevant factors of variation in the input data are aligned with individual neurons in the latent space. Validating the intuition, such representations have recently shown promising results in zero-shot transfer learning [16] and semi-supervised learning [8].

This thesis investigates the possible relationship between the two intriguing properties of neural networks outlined above: the counter-intuitive decision boundaries on one hand, and the apparent overly complex internal representations on the other. It is reasonable to assume the existence of such a connection, since the leading conjecture explaining the presence of adversarial examples posits that they come about due to excessive linearity of today's pattern recognizers [13]. However, models whose internal representations are disentangled are arguably less linear, since they are implicitly guided to capture the main generative factors of the data, which in datasets with enough complexity are non-linear with respect to inputs in the pixel space. This suggests that disentangled models could be less prone to be fooled by adversarial examples.

To test the preceding hypothesis, we empirically evaluated the robustness of state-of-the-art disentanglement-inducing VAEs to adversarial examples [1], and compared the results to regular, entangled VAEs. The analyses were carried out for the MNIST handwritten images dataset, as well as for CelebA, a large-scale dataset of celebrety faces. Surprisingly, it was found that disentangled generative models are actually *less* robust to attacks on both datasets, contradicting our initial rationale. This stands in stark contrast to previous work by Alemi et. al. [1], which performed similar analysis for supervised models, but arrived at the opposite conclusion, highlighting a fundamental difference between generative and discriminative models when it comes to adversarial examples.

The thesis is organized as follows. In chapter 1, a sufficiently in-depth overview of variational autoencoders, disentanglement, and adversarial examples is given. Chapter 2 outlines the experimental methodology, and provides exact details of the analyses done in this thesis for reproducibility. Chapter 3 gives the results of the experiments.

[1] In the context of generative models, an adversarial example is a datapoint which is very similar to the original, untampered image, but whose reconstruction differs markedly from the original's. As an example, an adversarial image could look like a regular depiction of the digit two, but which is reconstructed as the digit four by the generative model.

Chapter 2

Related work and background

This chapter introduces the preliminary topics that are integral to understanding the methods and results of this thesis. In addition, it provides an overview of the most important previous works that are closely related to ours. However, the reader is assumed to be comfortable with the basics of discriminative methods in machine learning. The first section of this chapter familiarizes the reader with a probabilistic approach to pattern recognition. The second section builds on the first, introducing the variational autoencoder. The third section focusses on how to regularize generative models such that the learnt representations would be disentangled. The last section introduces the general problem of adversarial examples, and discusses their applicability to generative models.

2.1 Probabilistic learning and inference

To fully appreciate variational autoencoders and the problems they are best suited to tackle, it is paramount to first be aware of the context that they operate in. To that end, a brief introduction to the probabilistic view of pattern recognition follows.

2.1.1 Discriminative approach

Usually, in the case of conventional supervised learning, one is concerned about capturing the probability distribution of some predefined labels, conditioned on a set of inputs. For example, in classification, we try to model the categorical distribution of possible classes, given an image (or some set of higher-level features derived from raw pixels) belonging to one of the categories. Relatedly, we could be interested in continuous conditional distributions, as one might be when trying to estimate the future earnings of a company based on its current key performance indicators.

As a concrete example, due to Bishop [5], of how viewing machine learning through a probabilistc lens can yield useful insights into well-known methodologies, let us see how the ubiquitous sum-of-squares error function comes about naturally from a principled probabilistic approach. Suppose we have N possibly high-dimensional training inputs $\boldsymbol{X} = \{\boldsymbol{x}^{(1)}, \boldsymbol{x}^{(2)}, \ldots, \boldsymbol{x}^{(n)}\}$, and

their corresponding one-dimensional target values $\mathbf{t} = \{t^{(1)}, t^{(2)}, \ldots, t^{(n)}\}$. Our uncertainty about the targets can be modelled as a Gaussian with a fixed precision β, whose mean is represented by a parameterized function $y(x, \boldsymbol{\theta})$ (e.g. a neural network):

$$p(t^{(i)}|\boldsymbol{x}^{(i)}, \boldsymbol{\theta}, \beta) = \mathcal{N}(t^{(i)}|y(\boldsymbol{x}^{(i)}, \boldsymbol{\theta}), \beta^{-1}).$$

If we further assume that the given targets were drawn independently from this normal distribution, we can estimate the unknown parameters $\boldsymbol{\theta}$ and β by maximizing the log-likelihood of the targets:

$$\begin{aligned}
&\arg\max_{\boldsymbol{\theta}} \log p(\mathbf{t}; \boldsymbol{\theta}) = \\
&\arg\max_{\boldsymbol{\theta}} \log \prod_{n=1}^{N} \mathcal{N}(t^{(n)}|y(\boldsymbol{x}^{(n)}, \boldsymbol{\theta}), \beta^{-1}) = \\
&\arg\max_{\boldsymbol{\theta}} \sum_{n=1}^{N} \log \mathcal{N}(t^{(n)}|y(\boldsymbol{x}^{(n)}, \boldsymbol{\theta}), \beta^{-1}) = \\
&\arg\max_{\boldsymbol{\theta}} \sum_{n=1}^{N} \log \left(\frac{\beta}{2\pi}\right)^{\frac{1}{2}} e^{-\frac{\beta}{2}(t^{(n)} - y(\boldsymbol{x}^{(n)}, \boldsymbol{\theta}))^2} = \\
&\arg\max_{\boldsymbol{\theta}} \sum_{n=1}^{N} \frac{1}{2}(\log\beta - \log 2\pi) - \frac{\beta}{2}(t^{(n)} - y(\boldsymbol{x}^{(n)}, \boldsymbol{\theta}))^2 = \\
&\arg\min_{\boldsymbol{\theta}} \sum_{n=1}^{N} (t^{(n)} - y(\boldsymbol{x}^{(n)}, \boldsymbol{\theta}))^2,
\end{aligned} \tag{2.1}$$

where the last equation follows from the fact that the first term inside the summation does not depend on the parameter $\boldsymbol{\theta}$, and that scaling the parameter-dependent term by a negative constant is equivalent to dropping the constant and turning the maximization problem into a minimization. With that, we have convinced ourselves that even in the usual discriminative setting, we are in fact making implicit use of a probabilistic approach to machine learning.

2.1.2 Generative approach

So far we have dealt with modelling the conditional distribution of the targets, given the inputs. Sometimes, however, we might be after the marginal distribution of the input data itself. Having such an object in hand, we are able to determine if an observed example has an unusually low probability of occurrence for anomaly detection [10], fill out missing dimensions of incomplete datapoints [11], or sample new, realistic datapoints from the learnt density function [21].

Capturing the marginal distribution of the inputs is often somewhat more involved than it was in the conditional case discussed previously. This is largely due the fact that high-dimensional, multi-modal datapoints have complex densities whose modelling with well-known distributions would yield suboptimal results. In such situations, additional structure is often incorporated into

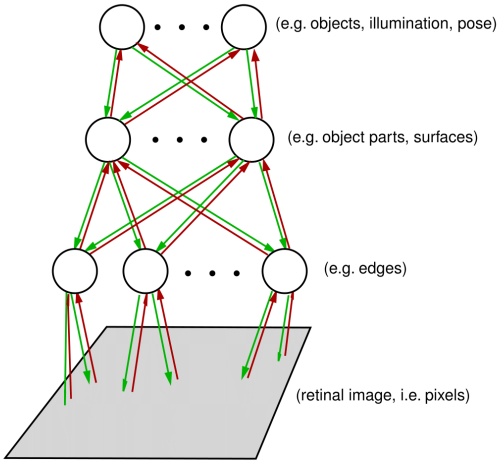

Figure 2.1: Illustration of a probabilistic model with latent variables. Green arrows represent the generative process, in which higher-level concepts guide the development of lower-level ones, eventually leading to the generation of each pixel in an image. Red arrows depict inference, in which case the goal it to infer the underlying causes of an obtained input.

the probabilistic model in the form of lower-dimensional latent variables.

The inclusion of such auxiliary variables is often motivated by the hierarchical nature of physical processes. For example, by thinking about how images could be constructed from a generative point of view, we might imagine that first it is decided which objects to lay onto the scene. Second, one might go into more detail and think about what individual parts do the objects consist of. Finally, the actual orientations of the edges might be decided upon, after which the actual imagine could be drawn out onto the canvas. Moreover, having imposed such hierarchical dependecy structure on our model, we can also traverse the dependency graph bottom-up, reducing our uncertainty about the latents, given an observed datapoint. This inversion of the generative process is called inference, and plays a central role in this thesis. Figure 2.1 illustrates the generative and inferential processes just described.

One immediate drawback to using more complicated latent variable models is that evaluating the likelihood turns out to be intractable, as one has to formally consider the probability of the observed datapoint under every possible setting of the latents. More specifically, consider an observable random variable $\boldsymbol{x}$, an unobserved latent $\boldsymbol{z}$, and their joint distribution $p_{\boldsymbol{\theta}}(\boldsymbol{x}, \boldsymbol{z})$, where the vector $\boldsymbol{\theta}$ denotes the parameters of the generative model [1]. Then, using the sum rule of probability, we can express the marginal of $\boldsymbol{x}$ as $p_{\boldsymbol{\theta}}(\boldsymbol{x}) = \int p_{\boldsymbol{\theta}}(\boldsymbol{x}, \boldsymbol{z}) d\boldsymbol{z}$.

[1] Note that we can focus on the marginal likelihood of individual datapoints, rather than the marginal likelihood of the whole dataset, since under the independence assumption, the former is composed of a sum of the latter (as shown in derivation 2.1): $\log p_{\boldsymbol{\theta}}(x^{(1)}, x^{(2)}, \ldots, x^{(n)}) = \sum_{n=1}^{N} \log p_{\boldsymbol{\theta}}(\boldsymbol{x}^{(i)})$.

Naturally, as we are unable to evaluate the likelihood function, explicit optimization of its monotonic tranform, the log-likelihood, presents difficulties as well. Fortunately, there exists a workaround, which entails optimizing a lower-bound of the log-likelihood instead. By introducing a new distribution $q_{\boldsymbol{\phi}}(\boldsymbol{z}|\boldsymbol{x})$, parameterized by $\boldsymbol{\phi}$, into our framework, we can lower-bound the original likelihood as follows:

$$\begin{aligned} \log p_{\boldsymbol{\theta}}(\boldsymbol{x}) &\overset{\text{sum rule}}{=} \\ \log \int p_{\boldsymbol{\theta}}(\boldsymbol{x}, \boldsymbol{z}) d\boldsymbol{z} &\overset{\text{multiply by identity}}{=} \\ \log \int p_{\boldsymbol{\theta}}(\boldsymbol{x}, \boldsymbol{z}) \frac{q_{\boldsymbol{\phi}}(\boldsymbol{z}|\boldsymbol{x})}{q_{\boldsymbol{\phi}}(\boldsymbol{z}|\boldsymbol{x})} d\boldsymbol{z} &\overset{\text{Jensen's inequality}}{\geq} \\ \int q_{\boldsymbol{\phi}}(\boldsymbol{z}|\boldsymbol{x}) \log \frac{p_{\boldsymbol{\theta}}(\boldsymbol{x}, \boldsymbol{z})}{q_{\boldsymbol{\phi}}(\boldsymbol{z}|\boldsymbol{x})} d\boldsymbol{z} &=: \mathcal{L}(\boldsymbol{x}; \boldsymbol{\theta}, \boldsymbol{\phi}). \end{aligned} \tag{2.2}$$

To see that this lower bound could indeed make the optimization problem easier, it helps to write it in two different forms. The first form illustrates that the lower bound can be written as the expected log-joint under the approximate posterior, plus an additive entropy term that does not depend on the parameters of the generative model:

$$\begin{aligned} &\mathcal{L}(\boldsymbol{x}; \boldsymbol{\theta}, \boldsymbol{\phi}) = \\ &\int q_{\boldsymbol{\phi}}(\boldsymbol{z}|\boldsymbol{x}) \log p_{\boldsymbol{\theta}}(\boldsymbol{x}, \boldsymbol{z}) d\boldsymbol{z} - \int q_{\boldsymbol{\phi}}(\boldsymbol{z}|\boldsymbol{x}) \log(\boldsymbol{z}|\boldsymbol{x}) d\boldsymbol{z} = \\ &\mathbb{E}_{\boldsymbol{z} \sim q_{\boldsymbol{\phi}}(\boldsymbol{z}|\boldsymbol{x})} \big[\log p_{\boldsymbol{\theta}}(\boldsymbol{x}, \boldsymbol{z}) \big] + \mathcal{H}(q_{\boldsymbol{\phi}}\big(\boldsymbol{z}|\boldsymbol{x})\big). \end{aligned} \tag{2.3}$$

The second form reveals that the free energy is nothing more than the original log-likelihood that we are lower-bounding, minus an additional penalty term which increases the gap between the bound and the log-likelihood in proportion to the distance between the approximate posterior and the real posterior, as measured by Kullback-Leibler divergence:

$$\begin{aligned} &\mathcal{L}(\boldsymbol{x}; \boldsymbol{\theta}, \boldsymbol{\phi}) = \\ &\int q_{\boldsymbol{\phi}}(\boldsymbol{z}|\boldsymbol{x}) \log \frac{p_{\boldsymbol{\theta}}(\boldsymbol{z}|\boldsymbol{x}) p_{\boldsymbol{\theta}}(\boldsymbol{x})}{q_{\boldsymbol{\phi}}(\boldsymbol{z}|\boldsymbol{x})} d\boldsymbol{z} = \\ &\int q_{\boldsymbol{\phi}}(\boldsymbol{z}|\boldsymbol{x}) \log p_{\boldsymbol{\theta}}(\boldsymbol{x}) + \int q_{\boldsymbol{\phi}}(\boldsymbol{z}|\boldsymbol{x}) \log \frac{p_{\boldsymbol{\theta}}(\boldsymbol{z}|\boldsymbol{x})}{q_{\boldsymbol{\phi}}(\boldsymbol{z}|\boldsymbol{x})} d\boldsymbol{z} = \\ &\log p_{\boldsymbol{\theta}}(\boldsymbol{x}) - \mathcal{D}_{\mathrm{KL}}\big(q_{\boldsymbol{\phi}}(\boldsymbol{z}|\boldsymbol{x}) || p_{\boldsymbol{\theta}}(\boldsymbol{z}|\boldsymbol{x})\big). \end{aligned} \tag{2.4}$$

Having laid out the two forms of the lower bound, one should notice that in equation 2.3, only the first term depends on the generative parameters $\boldsymbol{\theta}$, while in equation 2.4, the parameters of the approximate posterior feature only in the divergence term. This observation suggests a coordinate-wise optimization scheme where we take turns optimizing $\boldsymbol{\theta}$ and $\boldsymbol{\phi}$, leading us to the well-known Expectation-Maximization (EM) algorithm [11]. This approach is applicable when

we have analytically tractable forms for the expectation of the log-joint, as well as for the true posterior under the current generative parameters $\boldsymbol{\theta}$.

What makes EM particularly appealing is that each full step of the algorithm either increases the log-likelihood, or the algorithm has converged to the latter's local maximum. From equation 2.4, we see that free energy is maximized with respect to $\boldsymbol{\phi}$ when the KL vanishes (as it is always non-negative), which is accomplished when the approximate posterior [2]is set equal to the true posterior. After that, the lower bound is equal to the log-likelihood (under the current best-guess parameters). Since the next step, maximization with respect to $\boldsymbol{\theta}$ can not decrease the free energy, we observe from equation 2.4 that the log-likelihood can also not decarease, again due to the non-negativity of KL divergences.

Some of the latent variable models that have tractable expected log-joints and posteriors, yielding EM an appropriate tool for learning their parameters, include factor analysis, mixture of Gaussians, hidden markov models, and linear gaussian state-space models. However, often we are interested in using more complicated graphical models, particularly ones where continuous priors and conditionals have non-linear interactions. Assuming that we have the required derivatives of the lower bound in hand, one solutions would be to optimize the bound jointly using regular gradient-based methods. Keeping in mind that this approach is usually inferior to EM, as it loses the theoretical guarantees the latter provides, it is often the method of choice for handling models with intractabilities. A concrete example of such an approach is the variational autoencoder, the topic of the next section.

2.2 Variational autoencoders

2.2.1 General framework

As already alluded to in the previous section, the variational autoencoder is a model that optimizes the lower bound of the log-likelihood (equation 2.2) using a gradient-based optimization scheme. The form of the lower bound that it is explicitly working with is as follows:

[2]It is important to distinguish between the best-guess parameters that we are working with when carrying out the optimization scheme, and the maximum-likelihood parameters. Our objective is to find the latter, but we are always operating with an estimated set of parameters. When referring to the *true* posterior, we are not implying that we have access to the true, maximum-likelihood parameters, but the "true" form of the posterior, i.e. $p(x|z)$ as opposed to $q(x|z)$.

$$
\begin{aligned}
&\mathcal{L}(\boldsymbol{x};\boldsymbol{\theta},\boldsymbol{\phi}) = \\
&\int q_{\boldsymbol{\phi}}(\boldsymbol{z}|\boldsymbol{x}) \log \frac{p_{\boldsymbol{\theta}}(\boldsymbol{x}|\boldsymbol{z}) p_{\boldsymbol{\theta}}(\boldsymbol{z})}{q_{\boldsymbol{\phi}}(\boldsymbol{z}|\boldsymbol{x})} d\boldsymbol{z} = \\
&\int q_{\boldsymbol{\phi}}(\boldsymbol{z}|\boldsymbol{x}) \log p_{\boldsymbol{\theta}}(\boldsymbol{x}|\boldsymbol{z}) d\boldsymbol{z} + \int q_{\boldsymbol{\phi}}(\boldsymbol{z}|\boldsymbol{x}) \log \frac{p_{\boldsymbol{\theta}}(\boldsymbol{z})}{q_{\boldsymbol{\phi}}(\boldsymbol{z}|\boldsymbol{x})} d\boldsymbol{z} = \\
&\int q_{\boldsymbol{\phi}}(\boldsymbol{z}|\boldsymbol{x}) \log p_{\boldsymbol{\theta}}(\boldsymbol{x}|\boldsymbol{z}) d\boldsymbol{z} - \mathcal{D}_{\mathrm{KL}}(q_{\boldsymbol{\phi}}(\boldsymbol{z}|\boldsymbol{x}) || p_{\boldsymbol{\theta}}(\boldsymbol{z})) = \\
&\mathbb{E}_{\boldsymbol{z}\sim q_{\boldsymbol{\phi}}(\boldsymbol{z}|\boldsymbol{x})}\big[\log p_{\boldsymbol{\theta}}(\boldsymbol{x}|\boldsymbol{z})\big] - \mathcal{D}_{\mathrm{KL}}(q_{\boldsymbol{\phi}}(\boldsymbol{z}|\boldsymbol{x}) || p_{\boldsymbol{\theta}}(\boldsymbol{z})) \simeq \\
&\frac{1}{L}\sum_{l=1}^{L} \log p_{\boldsymbol{\theta}}(\boldsymbol{x}|\boldsymbol{z}^{(l)}) - \mathcal{D}_{\mathrm{KL}}(q_{\boldsymbol{\phi}}(\boldsymbol{z}|\boldsymbol{x}) || p_{\boldsymbol{\theta}}(\boldsymbol{z})), \quad \text{where } \boldsymbol{z}^{(l)} \sim q_{\boldsymbol{\phi}}(\boldsymbol{z}^{(l)}|\boldsymbol{x}),
\end{aligned}
\tag{2.5}
$$

where the first term of the last line is a Monte-Carlo estimate of the expectation above. The KL divergence is left as-is, because as we will soon see, for common distributions, it can be calculated analytically. In general, however, this term can be estimated by a finite set of samples as well.

An immediate problem that presents itself is that sampling directly from the approximate posterior is not a continuous operation. This presents a problem, as we need the gradient of the Monte-Carlo estimate of the lower bound with respect to $\boldsymbol{\phi}$ for optimization. In principle, the necessary gradients could be estimated using the score function estimator, an ubiquitious method in the reinforcement learning literature [30]:

$$
\begin{aligned}
&\nabla_{\boldsymbol{\phi}} \mathbb{E}_{\boldsymbol{z}\sim q_{\boldsymbol{\phi}}(\boldsymbol{z}|\boldsymbol{x})}\big[\log p_{\boldsymbol{\theta}}(\boldsymbol{x}|\boldsymbol{z})\big] = \\
&\int \nabla_{\boldsymbol{\phi}} q_{\boldsymbol{\phi}}(\boldsymbol{z}|\boldsymbol{x}) \log p_{\boldsymbol{\theta}}(\boldsymbol{x}|\boldsymbol{z}) d\boldsymbol{z} \overset{\text{multiply by identity}}{=} \\
&\int \frac{q_{\boldsymbol{\phi}}(\boldsymbol{z}|\boldsymbol{x})}{q_{\boldsymbol{\phi}}(\boldsymbol{z}|\boldsymbol{x})} \nabla_{\boldsymbol{\phi}} q_{\boldsymbol{\phi}}(\boldsymbol{z}|\boldsymbol{x}) \log p_{\boldsymbol{\theta}}(\boldsymbol{x}|\boldsymbol{z}) d\boldsymbol{z} \overset{\text{derivative of log}}{=} \\
&\int q_{\boldsymbol{\phi}}(\boldsymbol{z}|\boldsymbol{x}) \nabla_{\boldsymbol{\phi}} \log q_{\boldsymbol{\phi}}(\boldsymbol{z}|\boldsymbol{x}) \log p_{\boldsymbol{\theta}}(\boldsymbol{x}|\boldsymbol{z}) d\boldsymbol{z} = \\
&\mathbb{E}_{\boldsymbol{z}\sim q_{\boldsymbol{\phi}}(\boldsymbol{z}|\boldsymbol{x})}\big[\nabla_{\boldsymbol{\phi}} \log q_{\boldsymbol{\phi}}(\boldsymbol{z}|\boldsymbol{x}) \log p_{\boldsymbol{\theta}}(\boldsymbol{x}|\boldsymbol{z})\big] \simeq \\
&\frac{1}{L}\sum_{l=1}^{L} \nabla_{\boldsymbol{\phi}} \log q_{\boldsymbol{\phi}}(\boldsymbol{z}|\boldsymbol{x}) \log p_{\boldsymbol{\theta}}(\boldsymbol{x}|\boldsymbol{z}), \quad \text{where } \boldsymbol{z}^{(l)} \sim q_{\boldsymbol{\phi}}(\boldsymbol{z}^{(l)}|\boldsymbol{x}).
\end{aligned}
\tag{2.6}
$$

Unfortunately, due to its generality, the preceding estimator has a very high variance, rendering its use impractical in the context of generative modelling. Elaborate on the variance of the score function gradient estimator!

A better approach to estimating the variance, introduced concurrently by Kingma and Welling [19], as well as by Rezende et. al. [26], is to reparameterize the lower bound in equation 2.5 such that the necessary stochasticity that is injected into the model would not depend on any of its parameters. As a simple illustrative example of such an approach, suppose our approximate posterior is taken to be a univariate Gaussian: $z \sim p(z|x) = \mathcal{N}(\mu, \sigma^2)$. If we sampled z naively,

we would not be able to calculate the required derivatives of this random variable, neither $\frac{\partial z}{\partial \mu}$ nor $\frac{\partial z}{\partial \sigma}$. However, by reparameterizing the variable as $z = \mu + \sigma\epsilon$, where $\epsilon \sim \mathcal{N}(0, 1)$, we decouple the variables of our model from the stochasticity, resulting in differentiability: $\frac{\partial(\mu+\sigma\epsilon)}{\partial \mu} = 1$ and $\frac{\partial(\mu+\sigma\epsilon)}{\partial \sigma} = \epsilon$.

Let us denote the differentiable transformation of the random variable as $\boldsymbol{z} = g_{\boldsymbol{\phi}}(\boldsymbol{\epsilon}, \boldsymbol{x})$, where $\boldsymbol{\epsilon} \sim p(\boldsymbol{\epsilon})$ is the auxiliary noise variable that does not depend on the model's parameters. The lower bound of a mini-batch of M samples, randomly drawn from the full dataset, is then given by equation 2.7. In practice, Kingma and Wellig [19] found that the number of samples drawn from the approximate posterior can be taken to be 1 (i.e. $L = 1$), provided that the mini-batch is large enough. As the resulting bound is jointly differentiable with respect to $\boldsymbol{\theta}$ and $\boldsymbol{\phi}$, it can be optimized with any of the popular stochastic optimization methods, such as SGD, Adam [18], or RMSProp [29].

$$\begin{gathered}
\frac{1}{M}\sum_{i=1}^{M}\mathcal{L}(\boldsymbol{x}^{(i)};\boldsymbol{\theta},\boldsymbol{\phi}) = \\
\frac{1}{M}\sum_{i=1}^{M}\Big\{\mathbb{E}_{\boldsymbol{\epsilon}\sim p(\boldsymbol{\epsilon})}\big[\log p_{\boldsymbol{\theta}}(\boldsymbol{x}^{(i)}|g_{\boldsymbol{\phi}}(\boldsymbol{\epsilon},\boldsymbol{x}^{(i)}))\big] - \mathcal{D}_{\mathrm{KL}}(q_{\boldsymbol{\phi}}(\boldsymbol{z}|\boldsymbol{x}^{(i)})||p_{\boldsymbol{\theta}}(\boldsymbol{z}))\Big\} \simeq \\
\frac{1}{ML}\sum_{i=1}^{M}\Big\{\sum_{l=1}^{L}\log p_{\boldsymbol{\theta}}(\boldsymbol{x}^{(i)}|\boldsymbol{z}^{(i,l)}) - \mathcal{D}_{\mathrm{KL}}(q_{\boldsymbol{\phi}}(\boldsymbol{z}|\boldsymbol{x}^{(i)})||p_{\boldsymbol{\theta}}(\boldsymbol{z}))\Big\}, \\
\text{where } \boldsymbol{z}^{(i,l)} \sim g_{\boldsymbol{\phi}}(\boldsymbol{\epsilon},\boldsymbol{x}), \boldsymbol{\epsilon} \sim p(\boldsymbol{\epsilon}).
\end{gathered} \tag{2.7}$$

With that, we have laid out all the fundamental components that make up a variational autoencoder. The next subsection covers some of the specifics that are still left to be filled in, particularly the forms and parameteriztions of the distirbutions in play.

2.2.2 Specific example

The name "variational autoencoder" is usually reserved for a particular realization of the preceding framework, one where both the approximate posterior $q_{\boldsymbol{\phi}}(\boldsymbol{x}|\boldsymbol{z})$, as well as the conditional in the generative part of the model, $p_{\boldsymbol{\theta}}(\boldsymbol{z}|\boldsymbol{x})$, are parameterized by artificial neural networks. These distributions themselves are usually taken to be multivariate normals with diagonal covariances. The prior does not generally have learnable parameters, as it is taken to be an isotropic Gaussian: $p_{\boldsymbol{\theta}}(\boldsymbol{x}) = \mathcal{N}(\boldsymbol{z}; \boldsymbol{0}, \boldsymbol{I})$. Figure 2.2 gives a schematic of this setup.

A nice property that follows from having Gaussian distributions is the analytic tractability of the KL divergence featuring in the lower bound. Derive the corresponding closed-form equation.

Looking at the general outline of the model in figure 2.2, it becomes apparent why it is called an autoencoder. An input $\boldsymbol{x}$ is fed through a neural network, which outputs the mean and diagonal covariance of the approximate posterior. Making use of the reparameterization trick, a sample is then drawn from this distribution. As the the dimension of the latent variable is usually much

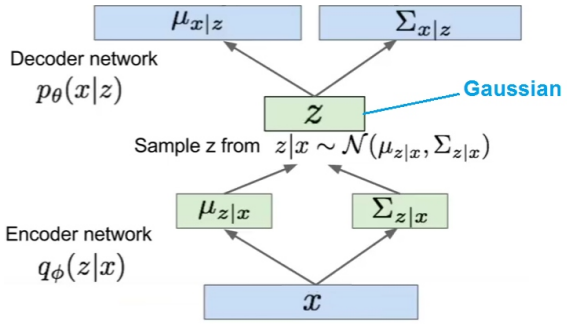

Figure 2.2: A schematic illustration of a variational autoencoder.

lower than that of the input, it is akin to the bottleneck layer of a regular autoencoder, and the whole underlying subnetwork (shown in green) is dubbed an encoder. The drawn vector $\boldsymbol{z}$ is subsequently fed through a second neural network, which outputs the estimated parameters of $p_{\boldsymbol{\theta}}(\boldsymbol{x}|\boldsymbol{z})$. As the estimated mean is obtained by upsampling the latent, and the conditional is maximized if it is equal to the original input, it bears resemblence to the decoding part of a conventional autoencoder, justifying the use of the name "decoder" for the underlying neural network.

2.2.3 Incorporating discrete variables

In the previous subsections, we focussed on variational autoencoders with continuous variables, namely ones with Gaussian distributions. Sometimes, however, it would be appropriate for the posterior to include some discrete variables as well. For example, when modelling handwritten digits, some of dimensions of the posterior could correspond to thickness, angle, size, and digit class. While the first three factor of variation are reasonably modelled by continuous distributions, a discrete one is more natural for the last. Unfortunately, the reparameterization trick that allowed joint optimization of the parameters in the Gaussian case is not applicable for discrete variables.

To get around taking direct samples from a discrete distribution, one might employ the Gumbel-Max trick [22]. Suppose our one-hot encoded random variable of interest, Y, has a discrete distribution with K choices, parameterized by unnormalized probabilities $(\alpha_1, \alpha_2, \ldots, \alpha_K)$, where $\alpha_i \in (0, \infty)$. A sample y can then be drawn from this distribution using the following scheme:

1. Draw K independent samples from a uniform distribution whose supported lies on the open unit interval: $U_i \sim \text{Uniform}(0, 1)$, where $i = 1, 2, \ldots, K$.
2. For each of the drawn samples, evaluate $x_i = \log \alpha_i + G_i$, where $G_i = -\log(-\log U_i)$ is a sample from the Gumbel distribution (hence the name of the trick).
3. Set $z_{\arg\max_i \{x_i\}}$ to 1, and all other dimensions of z to 0.

This looks promising, as the uniform distribution that we sample from does not depend on any of the parameters of the encoder. However, it is still of no use for our purposes, as we have now

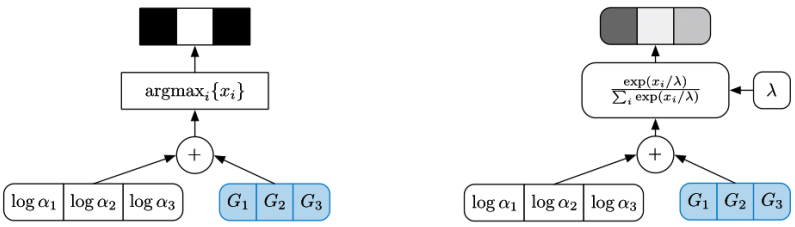

(a) Discrete(α) (b) Concrete(α, λ)

Figure 2.3: Concrete

introduced a non-continuous arg max operation. A solution, proposed concurrently by Maddison et. al. [23], and Jang et. al. [17], is to approximate it by a softmax function with a tunable temperature parameter $\lambda \in (0, \infty)$, as shown in Equation 2.8. Note that in this case, our sample, drawn from what the authors call a Concrete distribution, is no longer discrete, but rather a continous relaxation of it that approximates a one-hot vector as $\lambda \to 0$. The difference between the original Gumbel-Max trick, and its Concrete relaxation is illustrated in Figure 2.3.

$$z_i = \frac{\exp((\log \alpha_i + G_i)/\lambda)}{\sum_{j=1}^{K} \exp((\log \alpha_j + G_j)/\lambda)}. \tag{2.8}$$

Two additional considerations arise when Concrete variables are used in VAEs. First, since no gradients need to be computed at test time, the distributions can be discretized, allowing real categorical variables to be fed through the graph. Second, the KL term in the objective needs to be modified, as simply "plugging" the continous samples into discrete probability mass functions does not result in a valid KL divergence. This is because the samples are not drawn from the same distribution as is in the enumerator under the logarithm, as shown by Equation 2.9, where the Concrete posterior is denoted as $q^C_{\boldsymbol{\alpha},\lambda}$, while $q_{\boldsymbol{\alpha}}$ and $p_{\boldsymbol{\alpha}}$ stand for the approximate categorical posterior and prior, respectively:

$$\mathbb{E}_{\boldsymbol{z}\sim q^C_{\boldsymbol{\alpha},\lambda}(\boldsymbol{z}|\boldsymbol{x})}\Big[\log \frac{q_{\boldsymbol{\alpha}}(\boldsymbol{z}|\boldsymbol{x})}{p_{\boldsymbol{\alpha}}(\boldsymbol{z})}\Big]. \tag{2.9}$$

The authors of the original paper [23] provide several options for modifying the KL term, while arguing for replacing the discrete masses in the KL with Concrete densitites. However, unlike the Gaussian case, there is no closed form expression for the KL divergence between two Concrete distributions, so it is necessary to approximate it via sampling. However, for the types of models considered in this thesis, a variety of estimators have been found to exhibit too high of a variance, producing poor results as a consequence (Emilien Dupont, personal communication, August 1, 2018). Thus, we opted for replacing the original penalty with an analytic discrete KL term intead:

$$\mathbb{E}_{\boldsymbol{d}\sim q_{\boldsymbol{\alpha}}(\boldsymbol{d}|\boldsymbol{x})}\Big[\log \frac{q_{\boldsymbol{\alpha}}(\boldsymbol{d}|\boldsymbol{x})}{p_{\boldsymbol{\alpha}}(\boldsymbol{d})}\Big] = \sum_{i=1}^{K} q_{\boldsymbol{\alpha}}(d_i|\boldsymbol{x}) \log \frac{q_{\boldsymbol{\alpha}}(d_i|\boldsymbol{x})}{p_{\boldsymbol{\alpha}}(d_i)}, \tag{2.10}$$

where the vector $\boldsymbol{d}$ represents the one-hot categorical variable. While this strategy provides good results empirically, it is important to emphasize that the use of this KL term in the VAE objective does not necessarily result in a lower-bound of the marginal log-likelihood.

2.3 Disentangled representations

2.4 Adversarial examples

Chapter 3

Methods

Chapter 4

Results

Source	0	1	2	3	4	5	6	7	8	9
AS ignore-target	8.80%	82.58%	20.46%	16.52%	32.74%	43.58%	38.25%	40.10%	18.68%	64.22%
AS target	3.25%	34.05%	5.59%	6.15%	12.26%	10.88%	13.21%	11.85%	8.52%	19.30%

Table 4.1: Disentangled marginals

Source	0	1	2	3	4	5	6	7	8	9
AS ignore-target	5.87%	63.87%	11.49%	12.52%	64.10%	36.82%	26.99%	39.75%	16.21%	19.36%
AS target	1.88%	28.19%	3.24%	4.33%	13.48%	10.19%	8.81%	7.71%	5.71%	8.22%

Table 4.2: Entangled marginals

Source	0	1	2	3	4	5	6	7	8	9
AS ignore-target	3.21%	60.25%	7.43%	10.57%	53.79%	35.07%	25.06%	18.52%	23.28%	33.15%
AS target	0.86%	23.52%	1.46%	2.88%	10.88%	9.28%	6.34%	4.24%	8.24%	12.08%

Table 4.3: Entangled weight decay marginals

Chapter 5

Conclusion

Chapter 6

Appendix

Source	Targets									
	0	**1**	**2**	**3**	**4**	**5**	**6**	**7**	**8**	**9**
0	-	7.02% (0.00%)	9.80% (5.74%)	7.64% (4.29%)	9.62% (1.88%)	11.60% (5.86%)	8.63% (5.43%)	6.68% (0.10%)	9.45% (5.67%)	8.80% (0.31%)
1	99.16% (0.00%)	-	98.41% (93.66%)	95.32% (4.48%)	74.11% (44.89%)	94.50% (10.42%)	98.07% (26.55%)	23.25% (13.57%)	95.06% (73.08%)	65.31% (39.78%)
2	8.75% (1.01%)	23.32% (0.43%)	-	16.29% (5.93%)	25.75% (4.79%)	23.54% (1.58%)	6.86% (2.29%)	25.03% (12.78%)	26.04% (21.08%)	28.59% (0.44%)
3	3.23% (0.58%)	19.82% (0.34%)	16.09% (12.37%)	-	19.91% (0.81%)	16.50% (14.61%)	12.22% (1.90%)	19.39% (1.70%)	23.23% (18.40%)	18.29% (4.60%)
4	24.32% (0.37%)	42.75% (0.49%)	38.03% (24.18%)	28.12% (6.60%)	-	22.59% (4.10%)	19.77% (11.01%)	50.60% (7.13%)	34.12% (25.46%)	34.38% (30.99%)
5	46.78% (3.42%)	45.72% (0.92%)	64.34% (8.55%)	34.30% (26.49%)	30.23% (7.59%)	-	51.84% (11.15%)	41.29% (1.72%)	49.41% (31.49%)	28.35% (6.56%)
6	28.31% (6.89%)	34.79% (2.51%)	41.54% (32.64%)	37.96% (6.35%)	37.31% (22.98%)	32.55% (10.34%)	-	39.48% (2.40%)	49.02% (28.82%)	43.31% (5.98%)
7	46.96% (2.03%)	3.51% (0.11%)	38.03% (23.94%)	47.00% (2.54%)	37.46% (5.23%)	50.65% (5.63%)	43.61% (0.60%)	-	51.19% (29.52%)	42.53% (37.01%)
8	26.31% (0.91%)	13.01% (1.47%)	31.15% (25.29%)	23.31% (13.83%)	11.44% (5.95%)	20.38% (11.75%)	22.88% (6.85%)	10.97% (5.37%)	-	8.69% (5.26%)
9	80.48% (0.80%)	40.13% (1.77%)	79.96% (5.46%)	81.37% (22.60%)	38.78% (36.85%)	74.43% (24.06%)	75.00% (3.90%)	27.42% (20.96%)	80.37% (57.27%)	-

Table 6.1: Disentangled

Source	Targets									
	0	**1**	**2**	**3**	**4**	**5**	**6**	**7**	**8**	**9**
0	-	3.33% (0.00%)	8.67% (2.82%)	6.93% (2.10%)	6.33% (0.10%)	5.49% (1.83%)	4.80% (2.24%)	3.96% (0.00%)	9.04% (5.99%)	4.28% (1.88%)
1	60.50% (0.21%)	-	75.57% (51.43%)	71.26% (40.99%)	61.83% (24.38%)	66.78% (14.38%)	50.48% (18.72%)	62.99% (28.26%)	74.19% (56.95%)	51.22% (18.36%)
2	13.65% (1.53%)	4.04% (0.10%)	-	14.32% (11.05%)	10.55% (0.66%)	13.62% (0.24%)	10.94% (1.80%)	8.49% (1.15%)	16.67% (11.00%)	11.15% (1.61%)
3	8.89% (0.56%)	5.50% (0.11%)	8.79% (4.45%)	-	21.85% (0.33%)	14.23% (10.80%)	12.49% (0.57%)	5.60% (0.54%)	26.02% (19.91%)	9.30% (1.73%)
4	70.34% (2.76%)	42.32% (0.33%)	68.65% (9.35%)	89.19% (10.26%)	-	77.03% (4.84%)	23.84% (3.95%)	71.62% (4.77%)	75.28% (30.85%)	58.65% (54.19%)
5	34.34% (2.67%)	22.46% (0.25%)	47.30% (4.90%)	36.06% (24.04%)	36.29% (0.37%)	-	25.98% (6.62%)	36.05% (0.37%)	57.67% (43.56%)	35.26% (8.97%)
6	23.43% (16.49%)	7.59% (0.22%)	29.71% (7.35%)	42.27% (8.71%)	14.30% (6.60%)	24.36% (11.59%)	-	37.38% (0.00%)	41.28% (25.68%)	22.61% (2.61%)
7	33.44% (1.55%)	24.53% (0.32%)	29.70% (6.77%)	32.36% (15.10%)	53.05% (6.09%)	39.25% (1.22%)	55.95% (0.45%)	-	54.59% (8.72%)	34.88% (29.17%)
8	13.36% (1.03%)	7.41% (0.11%)	19.88% (8.44%)	34.31% (28.09%)	10.35% (1.25%)	22.35% (5.74%)	10.06% (1.73%)	18.65% (0.80%)	-	9.49% (4.23%)
9	8.41% (1.44%)	6.57% (0.32%)	32.33% (1.72%)	36.72% (20.34%)	14.97% (11.20%)	24.48% (7.67%)	7.81% (0.23%)	12.81% (6.35%)	30.10% (24.70%)	-

Table 6.2: Entangled

Source	Targets									
	0	**1**	**2**	**3**	**4**	**5**	**6**	**7**	**8**	**9**
0	-	2.22% (0.00%)	5.60% (1.27%)	4.95% (1.90%)	2.11% (0.00%)	4.15% (0.92%)	2.05% (1.08%)	1.68% (0.00%)	3.74% (2.14%)	2.40% (0.42%)
1	70.15% (2.19%)	-	75.69% (59.23%)	65.31% (24.92%)	39.46% (3.43%)	56.55% (8.51%)	39.42% (16.67%)	64.58% (50.20%)	78.83% (36.27%)	52.23% (10.24%)
2	8.79% (2.05%)	4.53% (0.11%)	-	6.61% (3.41%)	6.69% (0.68%)	9.53% (0.12%)	8.34% (1.16%)	7.46% (1.71%)	7.74% (3.35%)	7.19% (0.55%)
3	9.45% (1.08%)	5.85% (0.11%)	9.47% (6.47%)	-	14.82% (0.00%)	14.01% (9.51%)	12.02% (0.74%)	8.44% (2.43%)	9.60% (4.32%)	11.51% (1.27%)
4	54.66% (2.64%)	28.52% (1.62%)	57.04% (17.21%)	73.44% (5.99%)	-	74.53% (2.28%)	25.22% (3.95%)	60.29% (12.50%)	64.06% (10.97%)	46.33% (40.72%)
5	40.51% (13.69%)	20.58% (1.37%)	42.05% (3.56%)	32.15% (19.35%)	39.34% (0.69%)	-	33.92% (8.72%)	34.32% (6.89%)	37.85% (22.15%)	34.92% (7.09%)
6	18.98% (14.46%)	8.28% (1.20%)	35.20% (11.62%)	33.00% (3.51%)	15.51% (4.84%)	19.98% (5.52%)	-	31.84% (0.33%)	39.14% (14.33%)	23.60% (1.21%)
7	13.27% (1.72%)	7.84% (1.18%)	21.82% (11.18%)	18.72% (8.08%)	19.12% (1.04%)	18.45% (1.12%)	23.76% (0.12%)	-	29.38% (3.72%)	14.30% (10.01%)
8	19.11% (4.97%)	15.19% (1.42%)	37.68% (28.19%)	33.12% (18.57%)	16.25% (0.40%)	17.43% (3.86%)	25.20% (4.96%)	30.09% (6.18%)	-	15.43% (5.58%)
9	25.66% (2.89%)	16.65% (1.50%)	49.94% (11.74%)	56.67% (22.12%)	13.68% (6.49%)	37.21% (8.22%)	21.00% (0.49%)	38.96% (35.61%)	38.54% (19.69%)	-

Table 6.3: Entangled with weight decay

Bibliography

[1] Alexander A. Alemi, Ian Fischer, Joshua V. Dillon, and Kevin Murphy. Deep variational information bottleneck. *CoRR*, abs/1612.00410, 2016.

[2] Dzmitry Bahdanau, Kyunghyun Cho, and Yoshua Bengio. Neural machine translation by jointly learning to align and translate. *CoRR*, abs/1409.0473, 2014.

[3] Yoshua Bengio, Aaron C. Courville, and Pascal Vincent. Unsupervised feature learning and deep learning: A review and new perspectives. *CoRR*, abs/1206.5538, 2012.

[4] David Berthelot, Tom Schumm, and Luke Metz. BEGAN: boundary equilibrium generative adversarial networks. *CoRR*, abs/1703.10717, 2017.

[5] Christopher M. Bishop. *Pattern Recognition and Machine Learning (Information Science and Statistics)*. Springer-Verlag, Berlin, Heidelberg, 2006.

[6] Mariusz Bojarski, Davide Del Testa, Daniel Dworakowski, Bernhard Firner, Beat Flepp, Prasoon Goyal, Lawrence D. Jackel, Mathew Monfort, Urs Muller, Jiakai Zhang, Xin Zhang, Jake Zhao, and Karol Zieba. End to end learning for self-driving cars. *CoRR*, abs/1604.07316, 2016.

[7] G. Cybenko. Approximation by superpositions of a sigmoidal function. *Mathematics of Control, Signals and Systems*, 2(4):303–314, Dec 1989.

[8] Rodrigo de Bem, Arnab Ghosh, Thalaiyasingam Ajanthan, Ondrej Miksik, N. Siddharth, and Philip H. S. Torr. Dgpose: Disentangled semi-supervised deep generative models for human body analysis. *CoRR*, abs/1804.06364, 2018.

[9] Pratik Dubal, Rohan Mahadev, Suraj Kothawade, Kunal Dargan, and Rishabh Iyer. Deployment of customized deep learning based video analytics on surveillance cameras. *CoRR*, abs/1805.10604, 2018.

[10] Yaxiang Fan, Gongjian Wen, Deren Li, ShaoHua Qiu, and Martin D. Levine. Video anomaly detection and localization via gaussian mixture fully convolutional variational autoencoder. *CoRR*, abs/1805.11223, 2018.

[11] Zoubin Ghahramani and Michael I. Jordan. Supervised learning from incomplete data via an em approach. In J. D. Cowan, G. Tesauro, and J. Alspector, editors, *Advances in Neural Information Processing Systems 6*, pages 120–127. Morgan-Kaufmann, 1994.

[12] Ross B. Girshick, Jeff Donahue, Trevor Darrell, and Jitendra Malik. Rich feature hierarchies for accurate object detection and semantic segmentation. *CoRR*, abs/1311.2524, 2013.

[13] Ian Goodfellow, Jonathon Shlens, and Christian Szegedy. Explaining and harnessing adversarial examples. In *International Conference on Learning Representations*, 2015.

[14] Kathrin Grosse, Nicolas Papernot, Praveen Manoharan, Michael Backes, and Patrick McDaniel. Adversarial examples for malware detection. In Simon N. Foley, Dieter Gollmann, and Einar Snekkenes, editors, *Computer Security – ESORICS 2017*, pages 62–79, Cham, 2017. Springer International Publishing.

[15] Kaiming He, Xiangyu Zhang, Shaoqing Ren, and Jian Sun. Deep residual learning for image recognition. *CoRR*, abs/1512.03385, 2015.

[16] Irina Higgins, Arka Pal, Andrei A. Rusu, Loic Matthey, Christopher P Burgess, Alexander Pritzel, Matthew Botvinick, Charles Blundell, and Alexander Lerchner. Darla: Improving zero-shot transfer in reinforcement learning, 2017.

[17] Eric Jang, Shixiang Gu, and Ben Poole. Categorical reparameterization with gumbel-softmax. *CoRR*, abs/1611.01144, 2016.

[18] Diederik P. Kingma and Jimmy Ba. Adam: A method for stochastic optimization. *CoRR*, abs/1412.6980, 2014.

[19] Diederik P. Kingma and Max Welling. Auto-encoding variational bayes. *CoRR*, abs/1312.6114, 2013.

[20] Alex Krizhevsky, Ilya Sutskever, and Geoffrey E Hinton. Imagenet classification with deep convolutional neural networks. In F. Pereira, C. J. C. Burges, L. Bottou, and K. Q. Weinberger, editors, *Advances in Neural Information Processing Systems 25*, pages 1097–1105. Curran Associates, Inc., 2012.

[21] Anders Boesen Lindbo Larsen, Søren Kaae Sønderby, and Ole Winther. Autoencoding beyond pixels using a learned similarity metric. *CoRR*, abs/1512.09300, 2015.

[22] R. Duncan Luce. *Individual Choice Behavior: A Theoretical analysis*. Wiley, New York, NY, USA, 1959.

[23] Chris J. Maddison, Andriy Mnih, and Yee Whye Teh. The concrete distribution: A continuous relaxation of discrete random variables. *CoRR*, abs/1611.00712, 2016.

[24] Ari S. Morcos, David G.T. Barrett, Neil C. Rabinowitz, and Matthew Botvinick. On the importance of single directions for generalization. In *International Conference on Learning Representations*, 2018.

[25] Daniele Palossi, Antonio Loquercio, Francesco Conti, Eric Flamand, Davide Scaramuzza, and Luca Benini. Ultra low power deep-learning-powered autonomous nano drones. *CoRR*, abs/1805.01831, 2018.

[26] Danilo Jimenez Rezende, Shakir Mohamed, and Daan Wierstra. Stochastic backpropagation and approximate inference in deep generative models. In Eric P. Xing and Tony Jebara, editors, *Proceedings of the 31st International Conference on Machine Learning*, volume 32 of *Proceedings of Machine Learning Research*, pages 1278–1286, Bejing, China, 22–24 Jun 2014. PMLR.

[27] Adam Roberts, Jesse Engel, Colin Raffel, Curtis Hawthorne, and Douglas Eck. A hierarchical latent vector model for learning long-term structure in music. *CoRR*, abs/1803.05428, 2018.

[28] Christian Szegedy, Wojciech Zaremba, Ilya Sutskever, Joan Bruna, Dumitru Erhan, Ian J. Goodfellow, and Rob Fergus. Intriguing properties of neural networks. *CoRR*, abs/1312.6199, 2013.

[29] Tijmen Tieleman and Geoffrey Hinton. Lecture 6.5-rmsprop: Divide the gradient by a running average of its recent magnitude. *COURSERA: Neural networks for machine learning*, 4(2):26–31, 2012.

[30] Ronald J. Williams. Simple statistical gradient-following algorithms for connectionist reinforcement learning. *Machine Learning*, 8(3):229–256, May 1992.